Discrimination of Chiral Adsorption Configurations: Styrene on Germanium(100)

ARTICLE *in* THE JOURNAL OF PHYSICAL CHEMISTRY C · JANUARY 2009

Impact Factor: 4.77 · DOI: 10.1021/jp806308s

6 AUTHORS, INCLUDING:

Yun Jeong Hwang
Korea Institute of Science and Technology
47 PUBLICATIONS **978** CITATIONS
SEE PROFILE

Suklyun Hong
Sejong University
92 PUBLICATIONS **1,151** CITATIONS
SEE PROFILE

Article

Discrimination of Chiral Adsorption Configurations: Styrene on Germanium(100)

Yun Jeong Hwang, Eunkyung Hwang, Do Hwan Kim, Ansoon Kim, Suklyun Hong, and Sehun Kim

J. Phys. Chem. C, **2009**, 113 (4), 1426-1432 • Publication Date (Web): 05 January 2009

Discrimination of Chiral Adsorption Configurations: Styrene on Germanium(100)

Yun Jeong Hwang,[†] Eunkyung Hwang,[†] Do Hwan Kim,[†,‡,§] Ansoon Kim,[†,∥] Suklyun Hong,[*,§] and Sehun Kim[*,†]

Department of Chemistry and School of Molecular Science (BK 21), Korea Advanced Institute of Science and Technology, Daejeon 305-701, Republic of Korea, Division of Science Education, Daegu University, Gyeongbuk 712-714, Republic of Korea, Electronics and Telecommunications Research Institute, Daejeon 305-700, Republic of Korea, and Department of Physics and Institute of Fundamental Physics, Sejong University, Seoul 143-747, Republic of Korea

Received: July 17, 2008; Revised Manuscript Received: October 17, 2008

We investigated the adsorption geometries and desorption temperatures of styrene on a Ge surface using scanning tunneling microscopy (STM), temperature programmed desorption (TPD), and ab initio density functional theory (DFT) calculations. Our STM results show that styrene molecules attach via the vinyl group in two adsorption configurations: (i) on the top of single Ge dimers by forming di-σ bonds (OT) and (ii) in a paired end-bridge between two adjacent Ge dimers within the same dimer row (PEB). Moreover, the PEB configurations are divided into two types of adsorption configurations depending on the arrangement of the phenyl rings of the two styrene molecules: either the axis running through the two phenyl rings is diagonal to the dimer row direction (*trans*-PEB) or perpendicular to the dimer row direction (*cis*-PEB). STM images can discriminate the OT configurations with (*S*) and (*R*) chiralities, as well as the PEB configurations with diastereomeric (*R,S*) and enantiomeric (*R,R*) and (*S,S*) chiralities at the molecular level. The TPD measurements and DFT calculations show that the PEB configurations are thermodynamically more stable than the OT configurations because the chemisorbed styrene molecules desorb from Ge(100) at 320 K (OT) and at 365 K (PEB), respectively. Among the PEB configurations, STM results show that the *trans*-PEB configuration is more prevalent than the *cis*-PEB configuration at the initial coverage because of adsorbate-induced surface reconstruction. The *cis*- and *trans*-PEB configurations can induce phases with short-range order along the dimer row direction at high coverage of styrene.

1. Introduction

Recently, intense attention has been devoted to the organic functionalization of semiconductor surfaces for potential applications in chemical and biological sensors, thin film displays, and molecular devices.[1−7] Organic molecules on a semiconductor are prospective sites for applications, because various organic chemical reactions provide variation of their properties, such as size, shape, chemical reactivity, and conductivity. In particular, the adsorption of organic molecules containing a delocalized π-electron system[8−10] is important because of their reactivity with semiconductor surfaces and the applications of such molecules, particularly conducting polymers.[11,12] Styrene (C_6H_5−CH═CH_2) is one of the fundamental molecules containing a conjugated system, and its applications for molecular devices on a silicon surface have been proposed. Lopinski et al. reported that styrene molecules form a nanoscale molecular line on the hydrogen-terminated Si(100) surface via a spontaneous self-directed growth process.[13] The molecular line is suitable as a carrier channel because of the delocalized π states of styrene lying at the valence band edge.[14] Moreover, styrene adsorbed on the silicon surface has the potential to be a novel molecular resonant tunneling diode that shows negative differential resistance (NDR).[15,16] Therefore, studies on the adsorption of styrene on semiconductor surfaces are valuable in understanding the interaction of more complex organic molecules and for applications in new semiconductor devices.

In studies of organic molecules on semiconductor surfaces, various investigations have examined such molecules on the (100) surfaces of diamond, silicon, and germanium, all of which form similar surface X═X dimers (X = C, Si, or Ge). Many organic molecules can chemisorb on these surfaces via interactions between the functional groups of the organic molecules and the π bond of the surface dimers. To date, most of the studies have focused on Si surfaces,[3−5,17] with much less attention being paid to Ge surfaces.[1,7,18,19] However, research on Ge(100) is also important because such studies can be complementary to those on Si(100). They provide information about the influence of the lattice constants and the electronic structure of the surface on reactions with the adsorbate because the lattice constant of the Ge crystal is 4% larger, and the energy associated with buckling the Ge dimers (0.24 eV) is also larger than that for the Si dimers (0.06 eV).[20,21] It is known that dissimilarities between surface dimers cause different reactivities of molecules on Si(100) and Ge(100).[19,22] The Ge−C bond energy is 7∼9 kcal/mol smaller than that in Si−C, and many adsorption reactions of molecules on Ge(100) occur under thermodynamic control, in contrast to the preference for the kinetically controlled product in reactions on Si(100).[2,6,22−24]

Previous studies have found that styrene molecules adsorb on the Si(100)[15,25−28] and the Ge-covered Si(100)[29] surfaces mainly through the [2 + 2] cycloaddition reaction between the vinyl group of styrene and a single surface dimer. However,

* To whom correspondence should be addressed. E-mail: sehun-kim@kaist.ac.kr (S.K.); hong@sejong.ac.kr (S.H.).
† Korea Advanced Institute of Science and Technology.
‡ Daegu University.
§ Sejong University.
∥ Electronics and Telecommunications Research Institute.

10.1021/jp806308s CCC: $40.75
Published on Web 01/05/2009

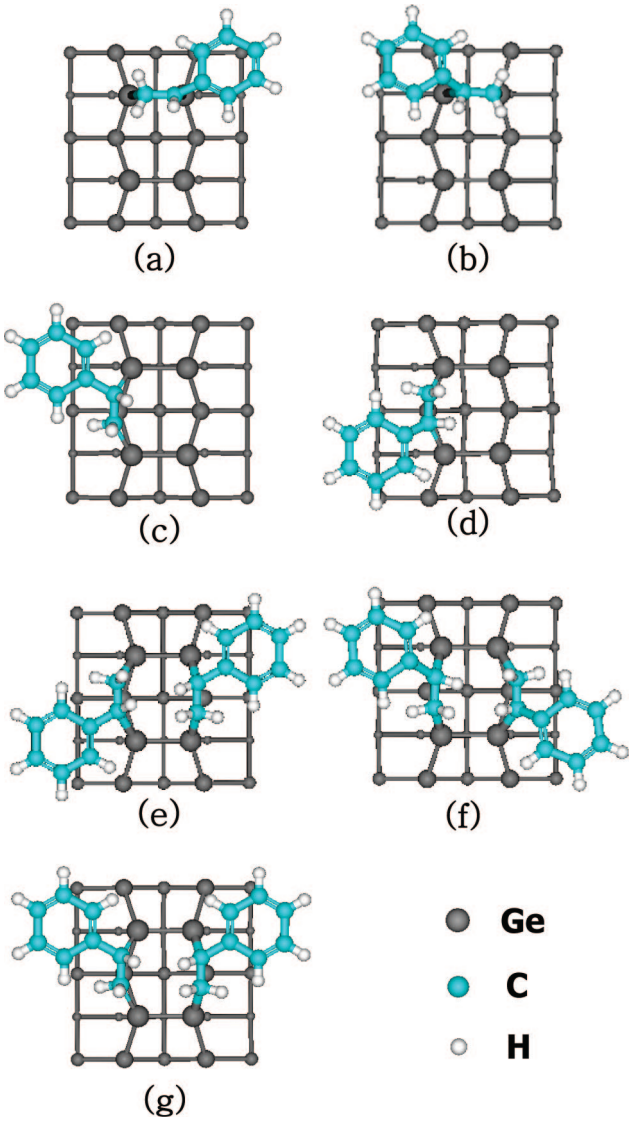

Figure 1. Possible bonding configurations of styrene chemisorbed on the Ge(100) surface: (a) (*S*) on top (OT), (b) (*R*) OT, (c) (*S*) chiral single end-bridge (SEB), (d) (*R*) chiral SEB, (e) (*R,R*) *trans* paired end-bridge (*trans*-PEB), (f) (*S,S*) *trans*-PEB, and (g) (*R,S*) *cis* paired end-bridge (*cis*-PEB) configurations.

the other possible adsorption configurations cannot be excluded on the Ge(100) surface. Even the simplest alkene, ethylene, chemisorbs on Ge(100) in two adsorption configurations: (i) on the top of a Ge dimer forming di-σ bonds (OT) and (ii) in a paired end-bridge between two adjacent Ge dimers within the same dimer row (PEB).[19,30−32] We expect that all of the adsorption configurations are formed via reaction of the vinyl group with Ge dimers because of the low reactivity of the phenyl ring, as in benzene on Ge(100) at room temperature (RT).[33] Figure 1 shows schematic configurations of the possible adsorption structures of styrene on the Ge(100) surface. Figure 1, parts a and b, shows that styrene adsorbs in the (*S*) and (*R*) chiral OT configurations, whereas Figure 1, parts c and d, shows that a single styrene molecule adsorbs in single end-bridge (SEB) configurations with (*S*) and (*R*) chirality, respectively, where it bridges either side of two adjacent dimers within the same dimer row. In addition, the PEB configurations can be divided into the (*R,R*)- and (*S,S*)-*trans*-PEB and (*R,S*)-*cis*-PEB depending on the orientation of the phenyl ring of the styrene, as shown in Figure 1e−g, respectively.

The chiral configurations of the organic molecules on the surface can be applied to chemical sensing, biological enzyme reactions, enantioselective antibody recognition, and heterogeneous asymmetric catalysis.[34,35] The chirality observed on the Si(100) surface has been found to originate from [2 + 2] and [4 + 2] cycloadditions between one alkene molecule and a surface dimer.[36−38] Recently, however, we reported that the dimeric chiral configuration of styrene molecules is mediated by Ge(100) surface dimers.[39]

In the present study, we examined the adsorption configurations of styrene on the Ge(100) surface at RT using scanning tunneling microscopy (STM), temperature programmed desorption (TPD), and density-functional theory (DFT). At the initial coverage, we could find the absolute chirality of the adsorbed styrene at the molecular level even though the styrene molecules have no stereoisomers themselves. From the TPD spectra and STM observations, the relative stability and population of each configuration are discussed in comparison with styrene/Si(100). The results are confirmed with theoretical calculations. The packing of adsorbed styrene at high coverage is also mentioned.

2. Experimental and Theoretical Methods

Experimental Details. The experiments were performed in two separate ultrahigh vacuum (UHV) chambers equipped with STM and TPD. The base pressure of the chamber was below 2.0×10^{-10} torr, which is low enough to maintain a clean surface for several hours.

A single crystalline Ge(100) wafer (n-type, Sb doped, $\rho <$ 0.4 Ω cm) was cut to a size of 2×10 mm^2 and mounted between two tantalum foil clips in a holder for resistive heating. The Ge(100) sample was cleaned by several cycles of Ar^+ sputtering (10 μA at 1.0 keV) at the sample temperature of T_s = 800 K, for 40 min, followed by annealing at T_s = 1000 K for 20 min. The cleanliness of the Ge surface was confirmed by STM.

Styrene (C_8H_8, 99% purity) purchased from Aldrich Chemicals was further purified through several freeze−pump−thaw cycles with dry ice until all dissolved gases were removed. The purity of the styrene was checked by quadrupole mass spectrometry (QMS), and styrene was directly dosed at RT through a doser with a seven-capillary array controlled by a variable-leak valve. The direct doser is adequate to reduce the chamber background pressure and contamination of the equipment by introduced styrene. The pressure in the chamber during introduction of styrene was maintained below 1×10^{-9} torr.

STM measurements were carried out at RT with an OMICRON VT-STM using electrochemically etched W-tips. All STM images were recorded in constant current mode with a tunneling current of I_t = 0.1 nA. Sample bias voltages (V_s) between V_s = −2.20 and +1.40 V were employed to obtain the images of the organic molecules effectively.

The TPD experiments were carried out in the UHV chamber equipped with a differentially pumped QMS. The Ge(100) surface was prepared as mentioned previously, and was positioned 2 mm away from the mass spectrometer aperture. For the low temperature (LT) TPD experiment, the Ge(100) sample was cooled with liquid nitrogen at 90 K, and the temperature was maintained while styrene was introduced and a spectrum taken. The surface temperature was monitored with a pyrometer and a chromel-alumel (type-K) thermocouple glued into the tantalum foil clips near the sample edge, the heating rate (β) being 1.5 K/s from 90 to 600 K. The desorption

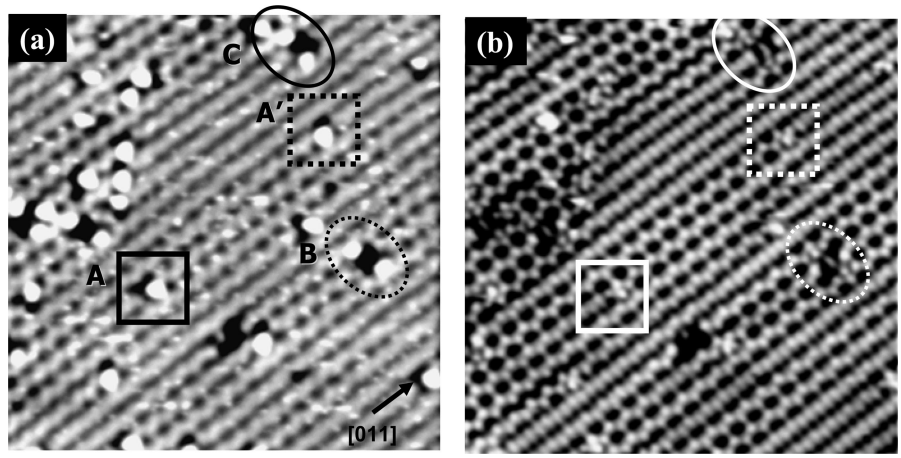

Figure 2. STM images (16×16 nm^2, $I_t = 0.1$ nA) of styrene adsorbed on a Ge(100) surface at a coverage of 0.02 ML: (a) an empty-state ($V_s = 1.0$ V) and (b) a filled-state ($V_s = -1.0$ V) STM image.

temperature of styrene was calibrated by the well-known desorption temperature (588 K) of hydrogen on the Ge(100) surface.[40]

Theoretical Calculations. To investigate the adsorption configurations of styrene on the Ge(100) surface, we performed ab initio calculations within the generalized gradient approximation (GGA) using the Vienna ab initio simulation package (VASP).[41,42] Plane waves up to an energy of 211.3 eV were included to expand the wave functions. Our slab model for the styrene adsorbed Ge(100) surface consisted of adsorbed styrene molecules, six Ge atomic layers, and an H passivating layer. The Ge bottom layer was passivated with two H atoms per Ge atom. We used a $c(4 \times 2)$, $p(4 \times 2)$, or a $p(4 \times 4)$ supercell with a $c(4 \times 2)$ surface symmetry. The surface structure was considered to be in equilibrium when the Hellmann−Feynman force was found to be smaller than 0.02 eV/Å. A Gaussian broadening with a width of 0.02 eV was used to accelerate the convergence in the k-point sum. Along with the use of self-consistent Kohn−Sham eigenvalues and wave functions, the constant-current STM images were simulated with the Tersoff-Hamann scheme.[43]

3. Results and Discussion

Figure 2 shows empty-state ($V_s = +1.0$ V, $I_t = 0.1$ nA) and filled-state ($V_s = -1.0$ V, $I_t = 0.1$ nA) STM images recorded simultaneously after the adsorption of ~0.02 ML styrene onto a clean Ge(100) surface at RT. As shown in Figure 2b, unreacted Ge dimers are imaged both as bean-shaped protrusions for the (2×1) structure or as zigzag chains for the $c(4 \times 2)$ structure depending on the buckling of the dimers. The STM images exhibit various adsorption features of styrene denoted as A, A′, B, and C.

Features A and A′ consist of a dark spot and one bright protrusion that are distinctively discriminated in the empty state. The dark spot is ascribed to the reacted vinyl group of styrene with the π bond states of the Ge dimer via formation of di-σ bonds. After adsorption of the styrene, lack of the π bond of the surface Ge dimer causes this region to be imaged as a dark spot compared with unreacted surface Ge dimers. In the case of the filled-state image shown in Figure 2b, however, the region of the dark spot in the empty state is hardly distinguishable from the bare Ge dimers because of narrowing of the bean-shaped protrusion. The spot attributed to the σ bond of C−C is bright in the filled-state STM image because the electronic density of the highest occupied states is expected to be high above the C−C single bond, similar to the OT configuration of ethylene molecules.[19] Simulated STM images within the perturbative Tersoff-Hamann approximation show the C−C σ bond of adsorbed ethylene brighter than the substrate in the filled-state STM image.[44] In addition, Ness et al. showed that the brightness of an adsorbed molecule depends on the distance between the tip and the sample. In the case of the silicon surface, a less polarizable adsorbate than the surface lessens the effect of the tip-induced electric field on the STM images,[44,45] and the adsorbate can appear brighter than the free dimers below a critical tip−sample distance (Z_{tp}). Therefore, the C−C σ bond of styrene reacting with the Ge(100) surface can be imaged brightly when the distance is below Z_{tp} because the molecule is less polarizable than the Ge(100) surface. In some cases, the C−C σ bond of styrene adsorbed on Ge(100) was imaged darker than free Ge dimers even in the filled-state image, similar to ethylene/Ge(100),[19] which can be explained if the STM tip distance is greater than Z_{tp} during the observation, depending on the condition of the tip.

The bright protrusion adjacent to the dark spot in features A and A′ in Figure 2a can be attributed to the phenyl ring of the styrene. Previous studies have shown that the aromatic ring images brightly[1] because the density of states located near the Fermi level for the π^* bond states of the aromatic ring increases the tunneling probability between the tip and the sample. This brightness suggests that the phenyl ring of styrene does not lose its aromaticity after the adsorption of styrene on the Ge surface; the styrene molecules attach to the Ge(100) surface through the vinyl group, and the phenyl group does not form a chemical bond with the surface.

We found that feature A′ is the mirror image of feature A. Depending on the direction of styrene relative to the Ge dimer, the OT configurations have either (*S*) or (*R*) chirality. We can discriminate the chirality of the OT configuration because the STM images precisely show the location of the C−C σ bond and the phenyl ring. Feature A is attributed to the (*S*) chiral OT configuration (Figure 1a), because the phenyl ring is located on the right of the Ge atom in the front dimer of the C−C σ bond-adsorbed styrene.

We observed that the neighboring dimers of the OT configuration are buckled (zigzag chain). This suggests either that the adsorption of styrene induces the buckling of Ge dimers, or that the adsorption of styrene preferentially occurs on the buckled $c(4 \times 2)$ structure rather than on other reconstructed surface sites such as $p(2 \times 2)$ or symmetric dimers. A series of

STM images recorded during the real-time dosing of styrene showed that the neighboring Ge dimers around the phenyl ring changed from symmetric to buckled dimers after adsorption. This change of buckling implies that the surface reconstruction is induced by the interaction with styrene, especially the phenyl group. We speculate that a repulsive interaction between the phenyl ring of styrene and the surface Ge atoms causes the nearest Ge atom to be a lower site of the buckled dimer, resulting in the $c(4 \times 2)$ reconstruction.

On the other hand, the next dimer of the C−C σ bond on the opposite side of the phenyl ring becomes symmetric, as shown in features A and A′ of Figure 2. The π bond states of the Ge dimer, whose charge transfer causes the buckling of the dimers, disappear after styrene is attached in the OT configuration. Therefore, the Ge dimer reacted with the vinyl group of styrene and the next dimer along the dimer row becomes a symmetric (bean-shaped) dimer. A similar surface reconstruction, where a buckled dimer changes into a symmetric dimer by adsorption, was also reported when hydrogen atoms doubly occupy the Ge dimer by breaking the π bond of the surface dimer.[46]

Meanwhile, we could also find other adsorption features denoted as B and C that have two bright protrusions (Figure 2). These features are twice as large as those of features A or A′. It is suggested that each of the features B and C consists of two styrene molecules and that the two bright spots at the ends of the features are associated with the phenyl ring of each styrene. Feature B might be thought of as two adjoining OT configurations whose phenyl rings are oriented opposite to each other. However, STM images for the OT configurations of ethylene on both Si(100) and Ge(100) show that the vinyl group prefers to adsorb on alternate dimer sites creating either a local (2×2) or $c(2 \times 4)$ structure below the 0.5 ML coverage region.[19,47,48] These previous studies point out that the repulsive interaction among the adsorbates prohibits adsorption on the adjacent dimer; thus it is unlikely that feature B is from two adjoining OT configurations.

Similarly to ethylene on Ge(100),[19] we expect that the styrene molecule can also adsorb in both the PEB and OT configurations. There are three distinctive features of PEB configurations depending on the orientation of the phenyl rings, as shown in Figure 1e−g. Feature B is attributed to the PEB configurations where the axis running through the two phenyl rings is oriented diagonal to the dimer row direction (*trans*-PEB). On the other hand, feature C corresponds to the PEB configuration where the axis running through the two phenyl rings is perpendicular to the dimer row direction (*cis*-PEB). The dark area between the two phenyl rings in features B and C in the empty-state STM image is attributed to two C−C σ bonds of the paired adsorbed styrene. Similarly to the OT configuration, these dark spots in the empty-state image appear bright in the filled-state image.

The *trans*-PEB configurations can be classified into (*R,R*)- and (*S,S*)-PEB configurations whose mirror plane is $\sigma_v = (0\ \bar{1}\ 1)$.[39] We can easily differentiate the two chiral products according to the direction of the *trans*-PEB configuration relative to the surface dimer row. Furthermore, both of the two chiral *trans*-PEB configurations are diastereomers of the (*R,S*)-*cis*-PEB configuration, that is, a nonchiral product. The *cis*- and *trans*-PEB configurations have different chiral properties due to their different symmetry point groups. In other words, the *trans*-PEB configuration is symmetric to the C_2 axis ([1 0 0]), perpendicular to the surface plane. On the other hand, the *cis*-PEB configuration has a mirror plane ($\sigma_v = (0\ \bar{1}\ 1)$), perpendicular to the surface plane and parallel to the dimer row direction. Therefore, the *cis*-PEB configuration is superimposable on its mirror image and is achiral, even though it contains chiral centers.

Figure 2 shows that the neighboring surface Ge dimers of the PEB configurations also convert into buckled dimers due to the interaction between phenyl rings and Ge atoms, similar to the case of the OT configuration. The buckled dimers induced by the *trans*-PEB configuration match well with a local $c(4 \times 2)$ domain, as shown in feature B, because the phenyl rings are placed diagonally. On the other hand, although the phenyl rings in the *cis*-PEB configuration also induce substrate buckling, neighboring surface dimers of the *cis*-PEB configuration have different surface reconstruction structures. As shown in feature C, although Ge dimers near the end of bright protrusion are buckled, those in the middle dimer row form symmetric dimers.

Even though a single-end-bridge (SEB) configuration is one of the possible configurations, we did not observe any features ascribable to it. Kim et al. reported that ethylene/Ge(100) does not have the SEB configuration due to less stability than the OT and PEB configurations.[19] The SEB styrene molecule breaks both partial π bonds of two adjacent dimers, resulting in highly reactive radicals or zwitterionic characters on the Ge dimer atoms that are not bonded to styrene. Therefore, we expect that the SEB exists only as an intermediate state in forming the PEB configuration, or it is too labile to obtain clear imaging with STM.

We have studied the thermal behavior of styrene molecules on Ge(100) using TPD. Figure 3a shows the TPD spectra of styrene molecules at $m/z = 104$ and their fragments at $m/z = 51$ ($C_4H_3^+$) and 78 ($C_6H_6^+$) attributed to the benzene fragments. When the Ge(100) surface was exposed to 1 L (1.0×10^{-6} torr·s) styrene at 90 K, the desorption peaks were observed at 170, 320, and 365 K; these peaks can be assigned to physisorbed molecules and two kinds of energetically separable chemisorbed molecules, respectively.

For the assignment of the chemisorption peaks, we compared the STM observation results after annealing. Sufficient styrene was introduced to saturate the Ge(100) surface at RT, followed by annealing at 340 K for 7 min. The surface was imaged after cooling it to RT. Figure 3b shows that styrene molecules remain only in the PEB configuration. Therefore, the desorption peak at 365 K is associated with styrene molecules in the PEB configurations. While we could find five adsorption configurations including two OT and three PEB configurations through experimental STM observations, only two chemisorption peaks were found in the TPD analysis. This implies that the thermal stabilities of some of the configurations are so similar that they cannot be discriminated by the TPD spectra.

The relative populations of the OT and PEB configurations vary depending on the sample annealing temperature, the dosing speed, and the sample bias voltage during imaging. Through real-time STM observations, we found a higher proportion of OT configurations compared with PEB configurations at higher dosing speed.

When we imaged the same surface region at submonolayer levels, the number of PEB configurations increased with time even though the increase in the coverage was negligible. Continuously taken STM images ($V_s = -1.0$ V, $I_t = 0.1$ nA) of the same surface region show that a new PEB configuration appears near a preadsorbed styrene molecule in the previously taken image. Styrene molecules that are not attached strongly enough can diffuse by the tip until they meet a second styrene and form the PEB configuration. Truncated images along the tip-scanning direction verify tip-induced desorption and diffusion of the styrene molecule on Ge(100). Once two styrene molecules

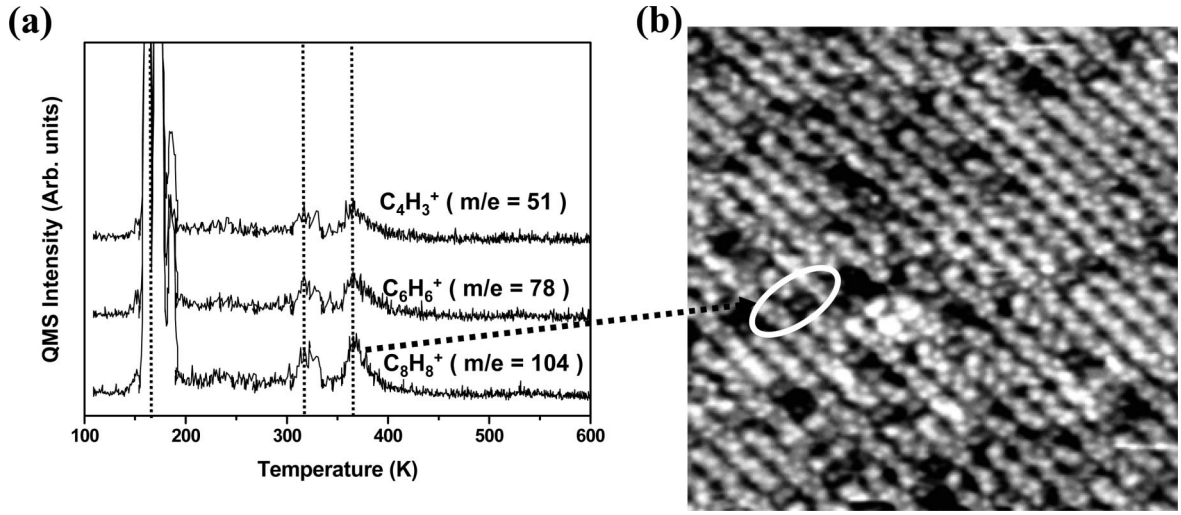

Figure 3. (a) TPD spectra of styrene ($m/z = 104$), and the fragments ($m/z = 51, 78$) and (b) a filled-state STM image (22×22 nm^2, $V_s = -1.00$ V, $I_t = 0.1$ nA) obtained at RT after annealing the Ge(100) surface saturated with styrene at 340 K for 7 min.

TABLE 1: Adsorption Energies E_{ads} (in eV/Molecule) of Relatively Stable Adsorption Geometries of Styrene on Ge(100) within the $p(4 \times 2)$ Unit Cell

			PEB	
configuration	OT	SEB	cis	trans
E_{ads}	0.93	0.71	1.65	1.74

adsorb as the PEB configuration, they do not move on the surface under mild imaging conditions ($V_s = -1.0$ V, $I_t = 0.1$ nA). Slower dosing provides sufficient time for the adsorbates to form the PEB configurations, causing the PEB configurations to be more populated.

When we recorded the STM images at $V_s = -1.60$ V during real-time dosing, a higher proportion of the PEB to the OT configuration was observed compared with real-time dosing at $V_s = -1.00$ V. Most of the adsorption structures are the PEB configuration with a few OT configurations at $V_s = -1.80$ V.[39] This behavior can be explained as follows: styrene is susceptible to STM tip-induced desorption via a resonant electronic excitation mechanism because the highest occupied molecular orbital (HOMO) level is located near the Fermi level.[49−51] At a sample bias voltage above the HOMO level of the Ge−C bond, the probability of tip-induced desorption or diffusion increases and the diffusing styrene molecules on Ge(100) might have more chance to undergo paired adsorption. Actually, we observed a truncated image of the OT configuration along the scanning direction and disappearance of the OT configuration while imaging the same surface region repeatedly at $V_s = -1.6$ V; however, the PEB configurations were not desorbed. All of these observations support the view that the PEB configuration is more stable than the OT configuration.

To elucidate the energetic aspects, we performed theoretical calculations on the possible configurations. Table 1 lists the adsorption energies of the configurations discussed above. The adsorption energy E_{ads} is defined as

$$E_{ads} = -[E_{tot}(\text{adsorbed}) - E_{tot}(\text{clean}) - E(\text{styrene})]$$

where E_{tot}(adsorbed), E_{tot}(clean), and E(styrene) are the total energies of the styrene-adsorbed surface, the clean $p(4 \times 2)$ surface, and the free styrene molecule, respectively. As in the case of acetic acid on Ge(100),[52] the OT configuration is more stable than the SEB configuration by 0.22 eV/molecule, shown in Table 1. However, subsequent addition of another styrene stabilizes the end-bridged adsorption geometry by leading paired end-bridged configurations. The PEB configuration will therefore be much more frequent than the SEB configuration. Experimentally, we did not find SEB structures, as discussed above. This energy trend is consistent with previous theoretical results.[53]

Figures 3b and 4 show that the populations of the *cis*- and *trans*-PEB configurations are not the same. The relative population of each chiral product is measured by directly counting the number of PEB configurations in the STM images at a coverage range of 0.05∼0.15 ML, where the PEB configurations are effectively distinguished. The average ratio of the PEB configuration populations is 1:1.4:1.4 (*cis*-PEB:(*R,R*)-*trans*-PEB:(*S,S*)-*trans*-PEB). From the relative populations among the PEB configurations, the *trans*-PEB configurations are expected to be more stable than the *cis*-PEB configuration. This is consistent with the theoretical results in Table 1. We found that *trans*-PEB is more stable than *cis*-PEB by 0.09 eV/molecule. The *trans*-PEB configuration is expected to be more stable than the *cis*-PEB configuration due to the different surface reconstruction induced by the adsorption configuration. As shown in Figure 2, the *cis*-PEB configuration diminishes the surface buckling of the middle dimer row, whereas the neighboring surface Ge dimers of either the (*R,R*)- or (*S,S*)-*trans*-PEB configurations are buckled as $c(4 \times 2)$ structures that are more stable surfaces than the (2×1) and $p(2 \times 2)$ structures. Formation of the more stable surface reconstruction may be the driving force preferentially leading to the *trans*-PEB rather than the *cis*-PEB configuration.

The most abundant experimental feature, B, seen in Figure 2 is compared with the theoretically simulated image for the most stable *trans*-PEB configuration (Figure 5). The experimental and theoretical results look very similar; hence we conclude that the *trans*-PEB configuration is the major adsorption structure at RT.

We observed packing of the PEB configuration at high coverage. Figure 6a shows the filled-state ($V_s = -1.40$ V, $I_t = 0.1$ nA) STM image recorded just after dosing with styrene at the saturation coverage. After the Ge(100) surface was scanned four times at high sample bias voltage ($V_s = -2.20$ V) in the same surface region, the filled-state ($V_s = -1.40$ V, $I_t = 0.1$ nA) STM image was recorded as shown in Figure 6b. Figure 6a is the saturated state with styrene. After scanning at high voltage, the packing phase of adsorbed styrene changed and a short-range ordered PEB configuration was observed along the

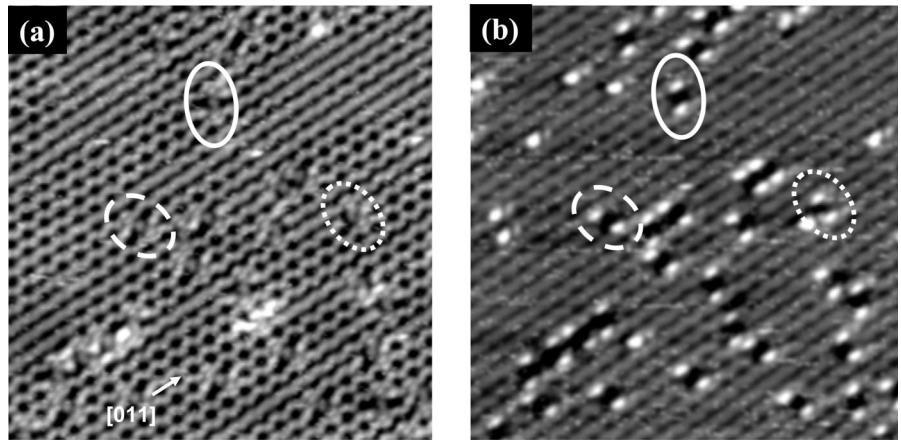

Figure 4. STM images (25 × 25 nm^2) of Ge(100) adsorbing styrene at a coverage of 0.07 ML: (a) a filled-state ($V_s = -1.0$ V) and (b) an empty state ($V_s = 1.0$ V) STM image. The solid line, the dash line, and dot line ellipses denote (*S,S*)-*trans*-PEB, (*R,R*)-*trans*-PEB, and *cis*-PEB configurations, respectively.

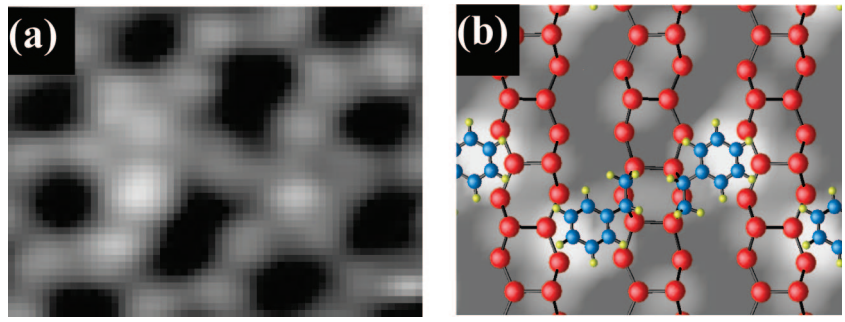

Figure 5. (a) Magnified filled-state STM image B in Figure 2b of styrene adsorbed on a clean Ge(100) surface and (b) the corresponding simulated image of the *trans*-PEB structure within $p(4 \times 4)$ unit cell.

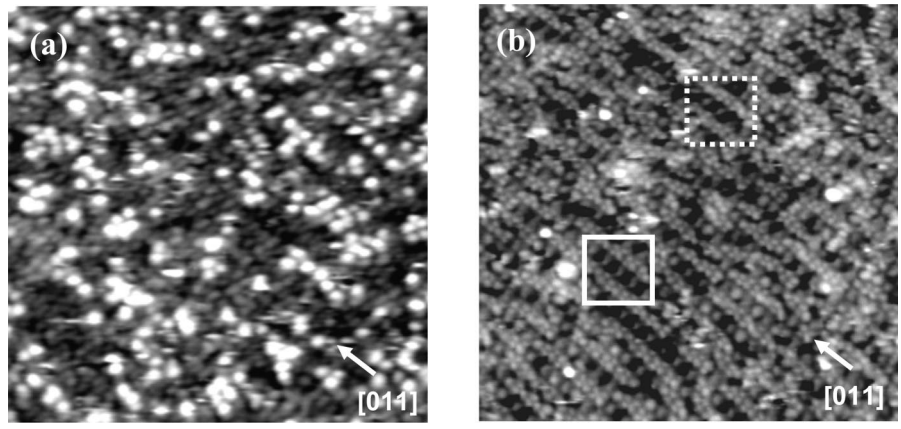

Figure 6. Filled-state (20 × 20 nm^2, $V_s = -1.40$ V, $I_t = 0.1$ nA) STM images of styrene on Ge(100): (a) STM image recorded just after dosing at saturation coverage and (b) STM image recorded in the same surface region after scanning four times at $V_s = -2.20$ V, $I_t = 0.2$ nA.

dimer row direction. As shown in Figure 6b, a dot box indicates the ordering of the *trans*-PEB configuration, and a solid box shows the ordering of the *cis*-PEB configuration. The *cis*-PEB configurations tend to form a longer PEB configuration line. The line profiles of the STM image show that the distance between two PEB configurations (8.16 Å) in the ordered phase is twice the interdimer distance (4.00 Å) within the same dimer row.[21] Figure 6b also shows that the PEB configuration lines are fabricated in alternative dimer rows; phenyl rings orient to the down Ge atom of the next dimer row, and adsorption of styrene molecules in the adjacent dimer row is prevented. Further studies on the control of homochiral chains and the ordered phase are required; the ordered phases of styrene have the potential for a carrier channel along the dimer row direction and enantioselective chemical reaction and sensing.

If a less stable OT configuration can be desorbed selectively by the STM tip, fabrication of the PEB configuration line will be more feasible. In the case of styrene on Si(100), tip-induced desorption was calculated. The applied energy initially produces phenyl ring excitation, and then ultimately leads to breaking of the Si−C bonds at sample biases in the $-2.40 \sim -3.00$ V range.[49] Although the electronic states of the styrene/Ge(100) hybrid system were not calculated, we expect that tip-induced desorption also occurs via a similar mechanism. Moreover, we expect that the styrene molecules adsorbed in the OT or PEB configurations may desorb at different sample bias voltages because we observed that at submonolayer levels the OT configuration is more mobile than the PEB configuration under $V_s = -1.60$ V. Desorption at different sample bias voltages of the OT and PEB configuration is possible if the HOMO level

of each configuration is different, depending on the adsorption geometries. The styrene molecules weakly adsorbed in the OT configuration are likely to be removed selectively, and the thermodynamically favorable PEB configurations remain as ordered phases for close packing, as shown in Figure 6.

4. Conclusions

We have investigated the chiral adsorption structure and thermal desorption behavior of styrene molecules on Ge(100) using STM and TPD. Styrene molecules, containing the vinyl group and phenyl group, exclusively adsorb on the Ge(100) surface via reaction between the vinyl group and Ge surface dimers. The phenyl group interacts with the surface Ge atom and induces buckling of the neighboring Ge dimers. Styrene molecules adsorb in two distinct adsorption configurations (OT and PEB). Depending on the attack direction of styrene to a Ge dimer, adsorbed styrene has either (R) or (S) OT configuration, whose chirality can be determined through high resolution STM images. The PEB configurations are divided into *cis*-PEB and *trans*-PEB configurations depending on the arrangement of the two phenyl rings, and these PEB configurations have two chiral centers. We can discriminate the enantiomeric (*R,R*)-, (*S,S*)-*trans*-PEB configurations and the (*R,S*)-*cis*-PEB configuration.

From the TPD spectra and theoretical calculations, we confirmed that the PEB configuration is thermodynamically more stable than the OT configuration. The more stable surface reconstruction of the neighboring Ge dimers makes the *trans*-PEB configuration more favorable than the *cis*-PEB configuration.

At the high coverage experiment, the *cis*- and *trans*-PEB configurations form short-range ordered phases along the dimer row direction. This ordering of the PEB configuration can be observed after selective desorption of the OT configuration by scanning the Ge(100) surface at $V_s = -2.20$ V.

Acknowledgment. This work was supported by the Brain Korea 21 Project, the SRC program (Center for Nanotubes and Nanostructured Composites) of MOST/KOSEF, the National R & D Project for Nanoscience and Technology, and Korea Research Foundation Grant No. KRF-2005-070-C00063. The calculations were supported by the KISTI through the Tenth Strategic Supercomputing Support Program. The work by A.K. was supported by the IT R&D program of MKE/IITA under Grant No. 2008-S-001-01 (Ubiquitous Health Monitoring Module and System Development).

References and Notes

(1) Cho, Y. E.; Maeng, J. Y.; Kim, S.; Hong, S. *J. Am. Chem. Soc.* **2003**, *125*, 7514.
(2) Filler, M. A.; Bent, S. F. *Prog. Surf. Sci. (U.K.)* **2003**, *73*, 1.
(3) Bent, S. F. *Surf. Sci.* **2002**, *500*, 879.
(4) Hamers, R. J.; Coulter, S. K.; Ellison, M. D.; Hovis, J. S.; Padowitz, D. F.; Schwartz, M. P.; Greenlief, C. M.; Russell, J. N. *Acc. Chem. Res.* **2000**, *33*, 617.
(5) Wolkow, R. A. *Annu. Rev. Phys. Chem.* **1999**, *50*, 413.
(6) Buriak, J. M. *Chem. Rev.* **2002**, *102*, 1271.
(7) Kim, A.; Maeng, J. Y.; Lee, J. Y.; Kim, S. *J. Chem. Phys.* **2002**, *117*, 10215.
(8) Lopinski, G. P.; Moffatt, D. J.; Wolkow, R. A. *Chem. Phys. Lett.* **1998**, *282*, 305.
(9) Hovis, J. S.; Hamers, R. J. *J. Phys. Chem. B* **1998**, *102*, 687.
(10) Qiao, M. H.; Cao, Y.; Deng, J. F.; Xu, G. Q. *Chem. Phys. Lett.* **2000**, *325*, 508.
(11) Bitzer, T.; Richardson, N. V. *Appl. Surf. Sci.* **1999**, *145*, 339.
(12) Vermeir, I. E.; Kim, N. Y.; Laibinis, P. E. *Appl. Phys. Lett.* **1999**, *74*, 3860.
(13) Lopinski, G. P.; Wayner, D. D. M.; Wolkow, R. A. *Nature* **2000**, *406*, 48.
(14) Hofer, W. A.; Fisher, A. J.; Bitzer, T.; Rada, T.; Richardson, N. V. *Chem. Phys. Lett.* **2002**, *365*, 129.
(15) Guisinger, N. P.; Greene, M. E.; Basu, R.; Baluch, A. S.; Hersam, M. C. *Nano Lett.* **2004**, *4*, 55.
(16) Guisinger, N. P.; Basu, R.; Greene, M. E.; Baluch, A. S.; Hersam, M. C. *Nanotechnology* **2004**, *15*, S452.
(17) Bent, S. F. *J. Phys. Chem. B* **2002**, *106*, 2830.
(18) Filler, M. A.; Mui, C.; Musgrave, C. B.; Bent, S. F. *J. Am. Chem. Soc.* **2003**, *125*, 4928.
(19) Kim, A.; Choi, D. S.; Lee, J. Y.; Kim, S. *J. Phys. Chem. B* **2004**, *108*, 3256.
(20) Jenkins, S. J.; Srivastava, G. P. *Phys. Rev. B* **1998**, *57*, 8794.
(21) Kubby, J. A.; Boland, J. J. *Surf. Sci. Rep.* **1996**, *26*, 61.
(22) Teplyakov, A. V.; Lal, P.; Noah, Y. A.; Bent, S. F. *J. Am. Chem. Soc.* **1998**, *120*, 7377.
(23) Wang, G. T.; Mui, C.; Musgrave, C. B.; Bent, S. F. *J. Phys. Chem. B* **2001**, *105*, 12559.
(24) Wang, Z.; Seebauer, E. G. *Appl. Surf. Sci.* **2001**, *181*, 111.
(25) Schwartz, M. P.; Ellison, M. D.; Coulter, S. K.; Hovis, J. S.; Hamers, R. J. *J. Am. Chem. Soc.* **2000**, *122*, 8529.
(26) Li, Q.; Leung, K. T. *J. Phys. Chem. B* **2005**, *109*, 1420.
(27) Basu, R.; Tovar, J. D.; Hersam, M. C. *J. Vac. Sci. Technol. B* **2005**, *23*, 1785.
(28) Calzolari, A.; Ruini, A.; Molinari, E.; Caldas, M. J. *Phys. Rev. B* **2006**, *73*, 125420.
(29) Zhang, Y. P.; Yang, L.; Lai, Y. H.; Xu, G. Q.; Wang, X. S. *Appl. Phys. Lett.* **2004**, *84*, 401.
(30) Miotto, R.; Ferraz, A. C. *Surf. Sci.* **2002**, *513*, 422.
(31) Lu, X.; Zhu, M. P. *Chem. Phys. Lett.* **2004**, *393*, 124.
(32) Cho, J. H.; Kleinman, L. *Phys. Rev. B* **2004**, *69*, 075303.
(33) Fink, A.; Menzel, D.; Widdra, W. *J. Phys. Chem. B* **2001**, *105*, 3828.
(34) Sholl, D. S.; Asthagiri, A.; Power, T. D. *J. Phys. Chem. B* **2001**, *105*, 4771.
(35) Smith, G. V.; Notheisz, F. *Heterogeneous Catalysis in Organic Chemistry*; Academic Press: San Diego, CA, 1999.
(36) Lopinski, G. P.; Moffatt, D. J.; Wayner, D. D. M.; Zgierski, M. Z.; Wolkow, R. A. *J. Am. Chem. Soc.* **1999**, *121*, 4532.
(37) Lopinski, G. P.; Moffatt, D. J.; Wayner, D. D. M.; Wolkow, R. A. *Nature* **1998**, *392*, 909.
(38) Lopinski, G. P.; Moffatt, D. J.; Wayner, D. D. M.; Wolkow, R. A. *J. Am. Chem. Soc.* **2000**, *122*, 3548.
(39) Hwang, Y. J.; Kim, A.; Hwang, E.; Kim, S. *J. Am. Chem. Soc.* **2005**, *127*, 5016.
(40) Lee, J. Y.; Maeng, J. Y.; Kim, A.; Cho, Y. E. *J. Chem. Phys.* **2003**, *118*, 1929.
(41) Kresse, G.; Furthmüller, J. *Comput. Mater. Sci.* **1996**, *6*, 15.
(42) Kresse, G.; Hafner, J. *J. Phys: Condens. Matter* **1994**, *6*, 8245.
(43) Tersoff, J.; Hamann, D. R. *Phys. Rev. Lett.* **1983**, *50*, 1998. Tersoff, J.; Hamann, D. R. *Phys. Rev. B* **1985**, *31*, 805.
(44) Ness, H.; Fisher, A. J. *Phys. Rev. B* **1997**, *55*, 10081.
(45) Ness, H.; Fisher, A. J. *Surf. Sci.* **1997**, *380*, L479.
(46) Maeng, J. Y.; Lee, J. Y.; Cho, Y. E.; Kim, S. *Appl. Phys. Lett.* **2002**, *81*, 3555.
(47) Shimomura, M.; Munakata, M.; Iwasaki, A.; Ikeda, M.; Abukawa, T.; Sato, K.; Kawawa, T.; Shimizu, H.; Nagashima, N.; Kono, S. *Surf. Sci.* **2002**, *504*, 19.
(48) Mayne, A. J.; Avery, A. R.; Knall, J.; Jones, T. S.; Briggs, G. A. D.; Weinberg, W. H. *Surf. Sci.* **1993**, *284*, 247.
(49) Patitsas, S. N.; Lopinski, G. P.; Hulko, O.; Moffatt, D. J.; Wolkow, R. A. *Surf. Sci.* **2000**, *457*, L425.
(50) Alavi, S.; Rousseau, R.; Lopinski, G. P.; Wolkow, R. A.; Seideman, T. *Faraday Discuss.* **2000**, 213.
(51) Alavi, S.; Rousseau, R.; Lopinski, G. P.; Wolkow, R. A.; Seideman, T. *Phys. Rev. Lett.* **2000**, *85*, 5372.
(52) Hwang, E.; Kim, D. H.; Hwang, Y. J.; Kim, A.; Hong, S.; Kim, S. *J. Phys. Chem. C* **2007**, *111*, 5941.
(53) Kim, H.; Cho, J. *J. Phys. Chem. C* **2007**, *111*, 5111.

JP806308S